



Characterization of Interlaminar Static and Fatigue Delamination Growth in Carbon/Epoxy Composites Reinforced with Carbon Nanotubes

Millan Kumar¹ · Pramod Kumar¹ · Shailendra Singh Bhadauria²

Received: 8 August 2022 / Accepted: 4 October 2023 / Published online: 16 November 2023
© The Author(s), under exclusive licence to Springer Nature B.V. 2023

Abstract

The present study focuses on the effect of CNT nanofillers on the interlaminar static and fatigue crack propagation in carbon fiber reinforced composite laminates. Multi-walled carbon nanotubes (MWCNTs) were dispersed over the laminate interface through solvent spraying technique. The mode I fracture toughness and R curve behavior were determined first from DCB specimens. Then, the fatigue tests were performed at different stress ratios for laminates containing different contents of CNTs to determine the delamination growth rate da/dN from fatigue crack growth (FCG) curves. When FCG curves are expressed as a function of G , where G is the energy release rate, the growth curves are dependent on the R -ratio. It was found that the addition of CNTs enhances the delamination resistance in the initial part of FCG curves, i.e. low cyclic region. As the test progresses, the effect gradually diminishes making nanofillers ineffective. It is then shown that the FCG curves can be characterized when crack growth rates are expressed as a function of the crack-driving force $\Delta\kappa$ used in the Hartman-Schijve equation. Therefore, the present paper presents a methodology to account for the stress ratio effect to evaluate the crack growth rate for any given R -ratio and to obtain a valid, upper-bound FCG rate curves in CNT reinforced laminates that exhibit high degree of scatter.

Keywords Delamination · Fiber reinforced composites · Fracture toughness · Fatigue crack growth · R -ratio · Nanoreinforcement

1 Introduction

Composites are widely used in aerospace industry, marine, wind energy, defence, construction sporting products, and automotive industry. The widespread application of composite materials will continually increase as the material becomes more affordable. Boeing 787

✉ Millan Kumar
kumar.milan19@gmail.com

¹ Department of Mechanical Engineering, Dr. B R Ambedkar National Institute of Technology, Jalandhar 144011, India

² Department of Industrial & Production Engineering, Dr. B R Ambedkar National Institute of Technology, Jalandhar 144011, India

aircraft has approximately 50% by weight composite parts in fuselage and wings and largest commercial Airbus A380 has 25% usage of composite materials [1]. Delamination is the primary mode of damage during the service life of aircrafts and repairing of in-service damage is essential to prevent disposal of its costly components. The purpose of the repairs is to maintain the structure's capacity to sustain design loads either through multiple load paths or slow crack growth approach which can be applied to single load path structures containing flaws at critical locations. When subjected to cyclic loading, damage may lead to catastrophic failure much earlier if the components are left unchecked. Hence design process when the component is subjected to cyclic loading is significant. However, the stochastic nature of fatigue makes it unpredictable since the accurate measurements of the in-service loads and environment conditions introduce uncertainty. This difficulty is worsened due to the fatigue crack growth (FCG) in a laminated composite being sensitive to small changes in loading conditions, e.g. R -ratio effect [2–6].

Composite structures contain flaws that can never be completely avoided and since the design should be such to ensure safe functioning the damage tolerance is an important factor in the design process. In this regard, damage tolerant design in composite laminates is considered as a crucial issue and for the last few decades significant research effort has been carried out to characterize the interlaminar FCG of fiber reinforced polymer (FRP) composites in the framework of linear elastic fracture mechanics [7–22]. A common design philosophy for critical applications is to adopt a no growth design in which delamination growth is required to be avoided altogether [23]. In “no growth” design approach an accurate value of the fatigue threshold is required associated with the particular damage state [24, 25]. In adhesives and composites, the FCG rate is generally more sensitive to load variations than for metals and as a result considerable scatter is often seen in the experimental FCG plots [26]. Therefore it is often the case that fatigue threshold becomes an important parameter with these materials. However, data obtained from full-scale fatigue tests in a number of examples, ‘F-111’, ‘A-320’, ‘F/A-18’ and Canadian ‘CF-5’ aircraft, have revealed the growth of small sub-millimeter initial delaminations or debonds that can grow when subjected to operational flight loads [23]. Therefore, the no-growth design approach cannot ensure that there will be no in-service debonding or delamination crack growth. The strict limitations of no-growth design approach have resulted in design practices allowing slow crack growth in the initial design which helps in determining the appropriate inspection intervals.

Slow crack growth approach is part of damage tolerant design philosophy that allows slow and predictable crack growth so that the planned inspections can be carried out. One application is in critical parts such as wing skin and fuselage skin to prevent skin cracks from spreading catastrophically. This approach to certifying adhesively bonded and composite structures was introduced by US Federal Aviation Administration (FAA) in 2009 [27] (Federal Aviation Authority. Airworthiness advisory circular No: 20-107B). This advisory circular enables a damage-tolerance design of delaminations and disbands found in-service composite materials and adhesively bonded joints in aircraft applications. However, one of the main requirements of this certification is that slow growth of cracks must be predictable. This is the one of main issues seen in composites that predictable growth under cyclic loads being not possible with high value of exponents using power law relationships. This puts limitations on the use of Paris relation since expressing da/dN as a function of ΔG , or G_{max} , has shortcomings [28, 29] such as:

- The dependence of both the proportionality constant and the exponent on the R -ratio.
- The dependence of both the proportionality constant and the exponent on the scatter associated with a given FCG test.

- Higher slopes in Paris relation resulting in large errors in the prediction of delamination growth rate since $da/dN \propto (P)^{2m}$.

Hence, power law relationships similar to Paris relation are not suitable for design purposes because of the large exponents [30, 31]. The realization that the Paris equation in composites, nanocomposites and adhesives can be extended to express da/dN as a function of energy release rate, subsequently led to the development of the Hartman-Schijve equation [6, 31, 32]. The Hartman-Schijve approach aims to give unique FCG curves for the fatigue data by taking into account the R -ratio effect [24, 25, 33]. ‘Short-crack’ effects could also be accounted for by the use of such unique and ‘master’ linear representation of the fatigue data [23, 34, 35]. Thus, it could be of great assistance to a designer for the prediction the crack growth rates.

The present study focuses on the effect of CNTs on the FCG rate of the CFRP laminates subjected to mode I static and fatigue loading. In this study, the effects of an (a) R -ratio, and (b) the scatter seen in the growth of both base and nanofiller reinforced laminates, are modeled using a form of the Hartman–Schijve crack-growth equation, which employs the term $\bar{\Delta}K$ as the crack driving force. It is shown that test data can be represented by using the Hartman-Schijve approach and that this formulation also takes into account the typical scatter seen in nanofiller reinforced carbon-epoxy laminates tests. This approach is proposed to characterize the interlaminar fatigue delamination growth in nanofiller reinforced laminates.

2 Materials and Methodology

2.1 Preparation of CNT/Carbon Fiber Reinforced Composites

In order to overcome the increased fabrication difficulty of CFRPs with the addition of nanofillers, several research groups [36–41] have worked on the development of techniques including direct deposition of nanofillers at the interlaminar region. In this work, a spraying method is used to introduce nanofillers into the composite laminates in order to improve the interlaminar toughness of a unidirectional composite. A solution of reinforcing nanofiller is spread between the laminate layers with an aid of airbrush. The air-brush spraying technique is used in this study, in which the CNT-solvent solution is directly sprayed on the interlaminar region. The vacuum bagging technique used in this study overcomes the limitations of fabrication using traditional resin infusion techniques such as vacuum assisted resin transfer infusion and resin transfer moulding. The resin infusion method generally needs a low viscosity resin for effective saturation of carbon fibers to reduce defects in the final composite part. However significant increase in the viscosity of matrix resin occurs with the addition of nanoreinforcements which leads to imperfect impregnation of the fibers [42, 43]. Moreover the uniform dispersion of CNTs into the bulk matrix like epoxy has been challenging due to strong Van der Waals interactions and large surface area of CNTs which leads to aggregation of nanofillers during mixing. The inevitable filtration of nanofillers during manufacturing may also lead to noticeable gradients in the nanoreinforcement distribution resulting in inferior quality of the composite part [44]. Therefore, in this study vacuum bagging method is preferred than traditional resin infusion techniques such as vacuum assisted resin transfer infusion (VARTI) and resin transfer molding (RTM).

The procedure for fabricating the panels of CNT/CFRP laminates involved three steps: CNT dispersion in a solvent, airbrush spraying of CNT-solvent solution, and finally vacuum bagging technique to fabricate laminates. Firstly, CNTs were dispersed in ethanol using the ultrasonication process for 30 min. CNTs have the tendency to entangle or agglomerate. Therefore, to improve the dispersibility of the CNTs in the solvent, the surfactant polyvinylpyrrolidone (PVP) was added in equal parts to the nanofillers. PVP prevents the agglomeration of CNTs and hence provides a stable solution. To disperse the nanofillers in the ethanol, sonication energy of 4000 J was applied to solution. Secondly, the CNT-ethanol solvent was sprayed on the mid-plane of the laminate with the help of an airbrush for better distribution of nanofillers. Since the gel time of epoxy used was limited, nanofiller solution had to be sprayed immediately. Thus, the ultrasonicated solution was filled in a spray gun as soon as the ultrasonication process was completed. The air pressure during the spraying operation was set at 30 psi (2.07 bar). The spray coating process used in study is presented in Fig. 1(a). Thirdly, a vacuum bagging process was used to fabricate the composite panels, as shown in Fig. 1(b).

The resin was applied by a brush to completely saturate the reinforcement and debulking was done using a roller after each layer applied. After all the fabric layers are stacked, peel cloth, perforated release film and bleeder cloth were placed over the preform. The perforated release film controls the amount of resin being soaked by bleeder cloth. A vacuum bagging film, tightly stretched to avoid any wrinkles, was placed over the mold to create leak-free system with the help of a sealant tape. Four pleats were created on the bagging film so that the stretched film under vacuum does not tear when it comes into contact with sharp sides of the enclosed contents. The air-suction line was connected to a vacuum pump and the set-up was enclosed.

The system was held under vacuum for 12 h to debulk the preform and remove any air voids in the laminate, as shown in Fig. 1(b). A valve was installed next to vacuum gauge on the air suction line which was closed when the vacuum pump was turned off. After 24 h the bagging consumables were torn apart to remove the laminate from the setup. The removed laminate part was further cured at room temperature for another 24 h before cutting them into DCB specimens.

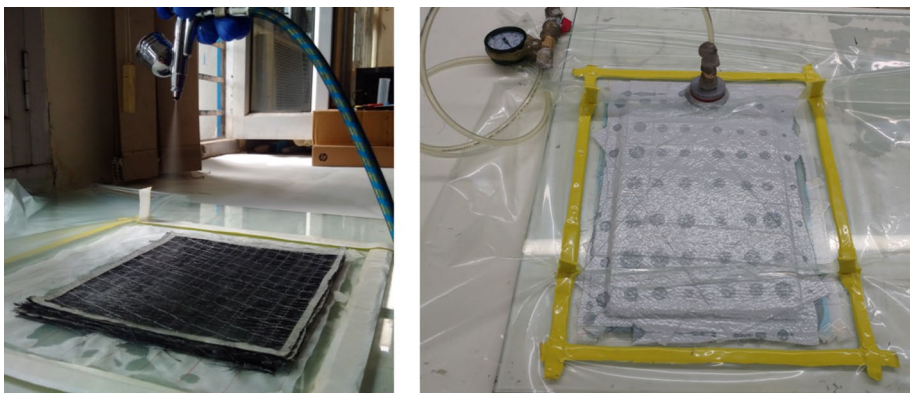


Fig. 1 a Airbrush spraying on interlaminar region b Vacuum bagging process

2.2 Specimen Preparation

The composite parts were fabricated with an approximate size 200 mm × 80 mm. The fabricated parts were cured at room temperature for 24 h and were cut into DCB specimens using a tungsten carbide hacksaw. A typical specimen size was 180 mm long by 25 mm wide with an insert film to create a starter delamination length of 50 mm. A 25 μm thick teflon release film was placed at the mid-plane of the composite layers in order to create an initial crack length of 50 mm for the mode I fatigue test. The thickness of the base laminate was 4.00 mm whereas the thickness for 0.05 wt%, 0.1 wt% and 0.5 wt% CNT laminates were 4.02 mm, 4.05 mm and 4.45 mm respectively. In total 20 samples were fabricated with 5 samples for each category of base laminate and CNT reinforced laminate for fracture toughness tests. For fatigue tests, twelve samples were prepared for testing under different *R*-ratios. Piano hinges were glued to the test samples to mount the samples on the machine grips. After abrading with emery paper and cleaning the surface with acetone, piano hinges were attached to the test samples using cyanoacrylate adhesive followed by another 24 h cure. One end of the plate was bolted to the hinge and the other end was mounted in the clamps of UTM.

3 Experimental Method

3.1 Fracture Toughness

Fracture toughness G_{IC} was measured for the DCB specimen according to ASTM standard D 5528. Test was started from the insert film as compared to starting it after precracking the specimen. Precracking was not done since the fiber-bridging effect affects the fracture toughness values. The fiber bridging behind the crack tip is considered an undesirable feature of unidirectional composites that does not occur in multi-directional lay-ups. Fiber-bridging phenomenon influences the curve shape of the plot of fracture energy G versus delamination increment Δa . Modified beam theory (MBT) was used to evaluate mode-I interlaminar fracture toughness. The correction factor Δ was evaluated to correct the value of fracture toughness by taking into account the shear deformation or displacement, and the rotation of the DCB arm at the crack tip. Compliance calibration fit for the base laminate was used to determine the correction factor Δ . Without this correction, the estimation of fracture toughness will be conservative and not suitable for design purposes. Fracture toughness was evaluated from the following relation:

$$G_{IC} = \frac{3P_c \delta_c}{2b(a + \Delta)} \quad (1)$$

where P_c , δ_c , and a and Δ are the critical applied load, displacement, crack length correction factor, respectively.

The displacement control mode was used in quasi-static tests with a displacement rate selected as 0.5 mm/min on ZWICK UTM. The lower value of displacement also helps in slowing the delamination growth rate in nanoreinforced composites so that sufficient measurements can be taken in spite of abrupt stages of delamination growth occurring sporadically from stick–slip behavior. A load cell of 10 kN was used for measuring the interlaminar load carrying capacity in the presence of a crack. The side section of the specimens

were smoothed using emery paper and applied with white correction fluid in order to observe the crack growth. A paper scale in millimeter units was attached to one side of the sample so that the images taken during the experimentation using a camera could be analyzed later in image processing software to determine the delamination length. Vertical marks were drawn extending from the paper scale to the sample so that measurements of delamination growth can be taken. The load and displacement were recorded every 0.1 s and the compliance was measured from these values. The improvements in the interlaminar fracture toughness, G_{IC} , caused by the introduction of nanoreinforcements using the spray method are compared, as reported in the literature, in Table 1.

3.2 Fatigue Crack Growth

The fatigue tests were conducted under displacement control on MTS hydraulic fatigue testing machine, as shown in Fig. 2. A frequency of 5 Hz was chosen for this study. The displacement control mode was preferred over load control because of the gradual reduction in cyclic load with delamination growth. Thus, as the test progress the SERR and hence da/dN decreases. The R -ratio of minimum to maximum displacement was set at 0.1, 0.5, and 0.9. The R -ratio is identical to displacement ratio ($\delta_{min}/\delta_{max}$) for linear elasticity and small deflections. Each specimen was loaded quasi-statically prior to fatigue testing to extend the crack to a few mm. Cyclic loading was started using the last displacement value from the quasi-static test [24].

The FCG method for composites and bonded joints is based on measuring the rate by which fatigue crack propagates (da/dN) and relating it to a suitable fracture mechanics parameter such as the stress intensity factor (K), SERR (G), or the J-integral [47]. In the case of composites and bonded joints, G has been the most commonly used fracture parameter in several studies [48–52]. The data, namely the minimum and maximum actuator displacements d_{min} and d_{max} , cycle number N and the minimum and maximum loads P_{min} and P_{max} , were recorded in a data file by specifying the frequency of the output. Specimens were tested until delamination growth rate had reached at least 1×10^{-6} mm/cycle. The system software recorded the output every 1000 cycles initially. The estimated delamination propagation rate was the determining factor on the selection of cycle count at which the test was interrupted after the first 10,000 cycles. With the test paused, a picture of the specimen from one side was taken while the actuator was held at d_{mean} . To evaluate the crack length, Image J software was then used to accurately locate the crack tip. Using this software, images were cropped to the area of interest and were converted to binary images. Then sobel filter was used to accurately pinpoint the location of crack tip.

Table 1 Effect of spray method for different nanofiller content on mode I strain energy release rate

Ref.	CNT Content	G_{IC}
[45]	7.5 g/m ²	10%
[46]	1.32 g/m ²	40% (onset) 32% (propagation)
[39]	0.05 wt%	24%
[40]	0.5 wt%	17%
[37]	0.047	47%
[36]	0.05	52%

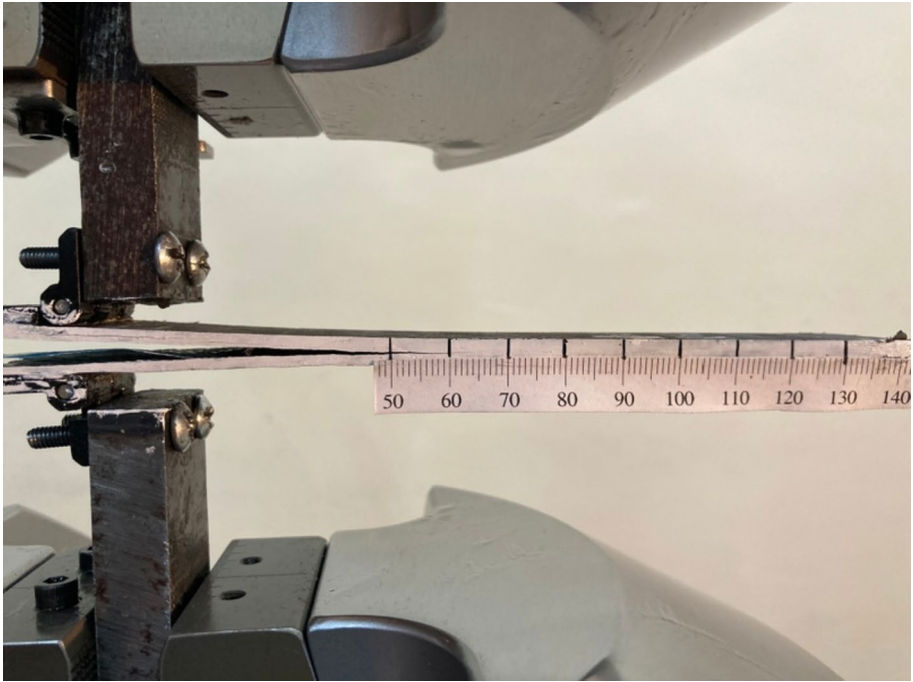


Fig. 2 Test set-up for delamination growth

The FCG curves are related to the SERR via a relationship similar to the Paris equation. Plots of $\log G_{max}$ against $\log da/dN$ yield a sigmoidal curve and the second phase of this curve defines a linear relationship between the G parameter and da/dN assuming a small-scale FPZ. Region I of the curve determines a value of fatigue threshold G_{th} , below which crack growth does not occur or the crack growth is so small that is immeasurable. In the second phase the FCG curve can be obtained by relationship similar to the Paris relation for metals [53] and is given as:

$$\frac{da}{dN} = C(G_{I_{max}})^m \quad (2)$$

where C and m are the material constants and da/dN is the increment in the crack length per cycle. The value of the exponent, m indicates the load sensitivity of the material that could result in variations in the crack propagation rate and is usually in the range of 1–3 for metals but tends to be higher for adhesives and FRP composites [26]. The Paris relation results here are plotted with maximum cyclic strain energy release rate, $G_{I_{max}}$. The use of ΔG_I has been shown in some studies to produce erroneous FCG curve, especially for lower R -ratios since the DCB arms typically come into contact during the unloading part of the cyclic loading that causes facial interference and crack closure. This causes artificially higher values of G_{min} , and hence lower value of ΔG [54, 55]. Consequently, FCG rates decrease resulting in conservative estimates. The crack growth rate, da/dN , was calculated using secant method (2 point technique). In this method, two points are connected with a straight line and the slope of this line represents the crack growth rate.

The fatigue dataset that has been experimentally obtained can be presented in a unique and linear representation by Hartman-Schijve approach. In principle, R -ratio effects and variations in data due to the addition of nanofillers can be accounted for with such a unique representation of the fatigue data. Therefore, it can be a great aid to a designer to predict the delamination growth rate in carbon fiber-epoxy laminates of unidirectional lay-up. Hartman–Schijve equation for composites in terms of SERR can be represented as:

$$\frac{da}{dN} = D(\overline{\Delta\kappa})^n \quad (3)$$

where the crack driving force is given as:

$$\overline{\Delta\kappa} = \left[\frac{\sqrt{G_I} - \sqrt{G_{Ithr}}}{\sqrt{\left\{ 1 - \sqrt{\frac{G_{Imax}}{A}} \right\}}} \right] \quad (4)$$

where G_{Ithr} is the threshold energy release rate. The G_{Ithr} is defined as the value of G corresponding to a fatigue crack rate of 10^{-7} mm/cycle. A threshold value is approximated when the average delamination growth rate da/dN decreases at constant applied load G_{max} . To find the G_{Ithr} for a full range of data, the experimental data has been extrapolated to 10^{-7} mm/cycle, which is taken due to the practical limit of measuring the crack extension. Hence for design purposes, a nominal or arbitrary value of fatigue threshold, which is based on expected number of cycles during the life of the structure, could be used. An appropriate safety factor could be used to decide the number of cycles.

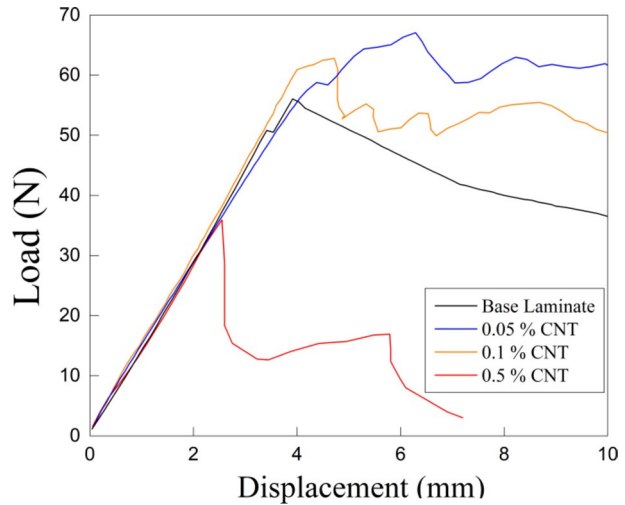
4 Results and Discussion

4.1 Mode I Fracture Toughness

Crack growth behaviour was measured using the DCB test specimen subjected to mode I loading. The specimens were 25 mm in width and contained the initial crack length of 50 mm. The typical mode I crack-growth resistance behavior of the various CFRP composites subjected to mode I quasi-static loading, is shown in Fig. 3. The base laminates show steady state crack growth behaviour in which crack growth rate is uniform.

In 0.05 wt% CNT-reinforced laminates, an increase in load was observed as soon as the crack propagation phase started that implies the enhancement in the stiffness of the interlaminar region of the laminate. In these laminates, the changes in crack growth rate occurs, which is commonly referred to as stick–slip behavior [56]. This trend can be observed on the load–displacement curve as there is a sudden drop in the force at-near constant displacement when the rapid crack growth occurs followed by crack arrest. During the phases of crack arrest, the load increases linearly according to the interlaminar stiffness of the specimen. Stick–slip behaviour in multiscale composites implies crack arrest in the presence of CNTs until further sufficient load is achieved from increase in test displacement for further crack propagation.

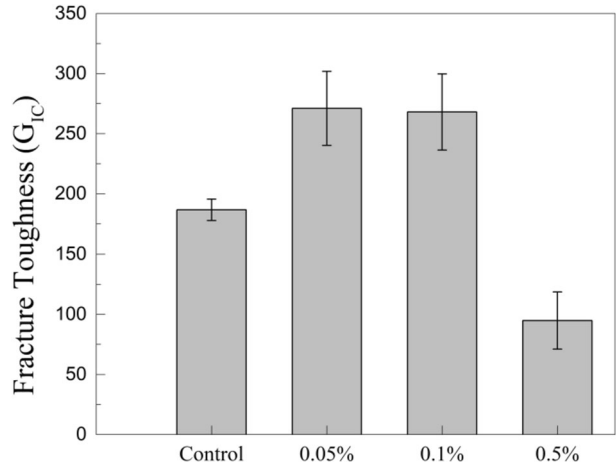
Fig. 3 Typical load displacement curves for base and multiscale hybrid composites



In 0.1 wt% CNT-reinforced laminates similar variations in load observed during the crack propagation phase were very frequent and which resulted in an unstable crack growth. This means 0.1 wt% CNT reinforced laminate exhibited more stick slip behaviour as compared to 0.05 wt% CNT laminate. Moreover the lower load–displacement values during the crack propagation phase means the strain energy release rates during the propagation phase are much lower as compared to 0.05 wt% CNT laminates. In this case the addition of higher content of CNTs introduced weak points in the interlaminar region and the further adverse effect of this on the adhesion between the fibers and the matrix caused decrease in the fracture energy. The stick–slip can occur sporadically in between stages of steady state delamination propagation in which multiple small reductions in load take place (0.1 wt% CNT) or it can occur during the entire propagation test in which large reduction of load take place at a single displacement value (0.5 wt% CNT). For 0.5 wt% CNT laminates, at critical load and displacement, there is a sudden reduction in load at almost constant displacement. This is due to the rapid growth of delamination indicating poor fiber–matrix adhesion–resulting in reduced interlaminar toughness at higher quantity of nanofillers. It was followed by stick–slip behavior exhibited by the increasing load but the interlaminar stiffness of the laminate was already reduced significantly at such lower load levels. The average fracture toughness for the base CFRP laminate was 180.6 J/m^2 , whereas its values were 270.92 J/m^2 , 268.27 J/m^2 and 94.8 J/m^2 for the 0.05 wt %, 0.1 wt % and 0.5 wt % CNT reinforced laminates, as shown in Fig. 4. The standard deviations for nanofiller reinforced laminates were high as compared to base laminates and this limitation may prove to be a disadvantage considering the high cost of the set-up involved. The fracture toughness is highly dependent on the distribution of nanofillers at the crack front and any small variation in that distribution could affect the fracture toughness values significantly.

The fracture energy depends on the degree of fiber-bridging, and its trend as observed in Fig. 5 corresponds to the steepness of the curves in R curves ("R" for resistance). R -curves are differentiated as steep (large difference) or flat (small difference) depending on the variation between initiation and plateau values of SERR. Fracture energy (SERR) versus delamination length plot starts with the initial G value, which increases with crack increment and finally reaches a near-constant plateau value. The strain energy release rate, G_I ,

Fig. 4 Mode I fracture toughness for base and nano-reinforced composites



for base laminate increased over the initial 10 mm of crack propagation and then reached a plateau. For both 0.05 wt% and 0.1 wt% CNT laminates the plateau reaches about after 17 mm of delamination growth. This is known as “R-curve” behaviour in which the fiber bridging in the mid-plane of the laminate results in near constant plateau value.

Fracture toughness and propagation are highly affected by fiber bridging in which the intermingled carbon fibers behind the crack tip are not separated with crack propagation. For 0.05 wt% CNT laminate, as shown in Fig. 6(a), the fiber bridging is very dominant which in conjunction with the effect of CNT bridging result in the highest improvement in G_{IC} . The bridged fibers increase the apparent fracture toughness as the fibers in the interlaminar region fail to separate and bridge the crack as it progresses. Once the bridged fibers break, fracture energy is released which is associated with debonding of the larger surface area of the bridged fibers. In 0.1 wt% CNT reinforced laminates, CNTs inhibit the

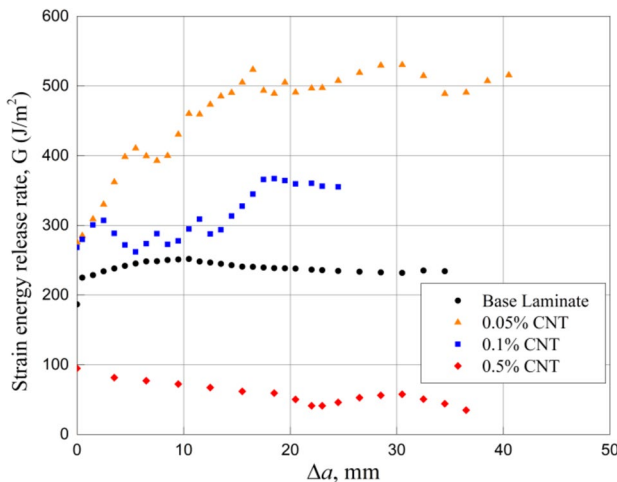


Fig. 5 Resistance curves for various laminates

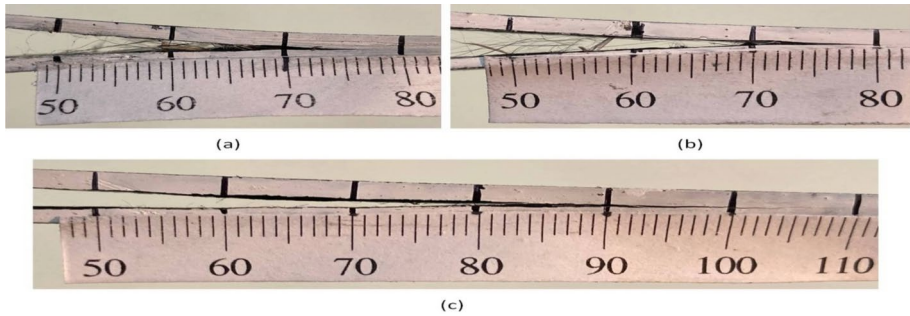


Fig. 6 Extent of fiber bridging: **a** 0.05% CNT; **b** 0.1% CNT; **c** 0.5% CNT laminate

interaction between the crack and the fabric since nanofillers act as obstacles for crack to migrate to the fabric, which leads to apparently lower amount of fiber bridging, as shown in Fig. 6(b). This implies that higher quantity of CNTs suppress the degree of fiber bridging to some extent, which results in lower values of average initiation and propagation toughness. A crack propagating through the CNT-reinforced interlaminar region, without any fiber bridging, would be expected to exhibit a lower fracture energy as observed. The case of 0.5% wt CNT composite exhibits no fiber bridging due to high amount of nanofillers inhibiting the interaction between the crack and the fabric.

4.2 Interlaminar Fatigue Crack Growth

The fatigue delamination growth is characterized using specimens similar to those used to characterize delamination under monotonic loading. DCB specimens with a crack length of 50 mm were used for the investigation of delamination growth under mode I loading by evaluating the delamination growth per fatigue cycle, da/dN as a function of G . The SERR was computed from the load, displacement, and the crack length measurements at regular intervals during the experimentation. Prior to starting the fatigue test, each specimen was quasi-statically loaded to generate a pre-crack of few mm long. Stelzer and co-workers proposed a method in which the last value of displacement is chosen, i.e., cyclic loading is started using the last displacement value from the quasi-static test [25]. Data has been represented as a function of $G_{I_{max}}$ in Paris relationship. The test input, as shown in Table 2 lists specimen type, applied stress ratio, maximum applied SERR $G_{I_{max}}$.

The FCG curves obtained from the fatigue test data of the base laminates is shown in Fig. 7. For the base laminate with increasing R -ratio, the slopes of these curves obtained were rather steep. The lower stress ratio resulted in much higher crack growth rate in the beginning of the tests and this effect diminished at higher stress ratio of 0.9. The crack closure effect was present for lower R -ratios resulting in breakage of fibers that bridge the crack faces. At lower stress ratio, the higher displacement of the DCB arms resulted in crack closure during the unloading part of the cycle. This effect results in bridged fibers being broken behind the crack tip resulting in lesser energy required for further delamination propagation. Since the amount of fiber breakage increases by the amount crack closure takes place, the SERR for subsequent delamination propagation reduces for lower R -ratios. Therefore, at different R -ratios the differences between the various FCG curves increases as the experiment progressed. In tests with higher R -ratios, the value of $G_{I_{max}}$ was relatively

Table 2 Test input for fatigue delamination growth tests

Specimen	Stress Ratio (<i>R</i>)	Applied $G_{I_{max}}$ (J/m ²)
Base Laminate	0.1	212.81
	0.5	204.68
	0.9	181.24
0.05% CNT	0.1	275.44
	0.5	269.82
	0.9	267.24
0.1% CNT	0.1	266.27
	0.5	252.71
	0.9	270.78
0.5% CNT	0.1	105.5
	0.5	92.85
	0.9	87.38

smaller at the start of the tests, which didn't reduce greatly with subsequent crack growth, resulting in high slope values implying rapid decrease in da/dN as the test progressed. The fitting parameters C and m for the FCG plots of Paris relation are presented in Table 3.

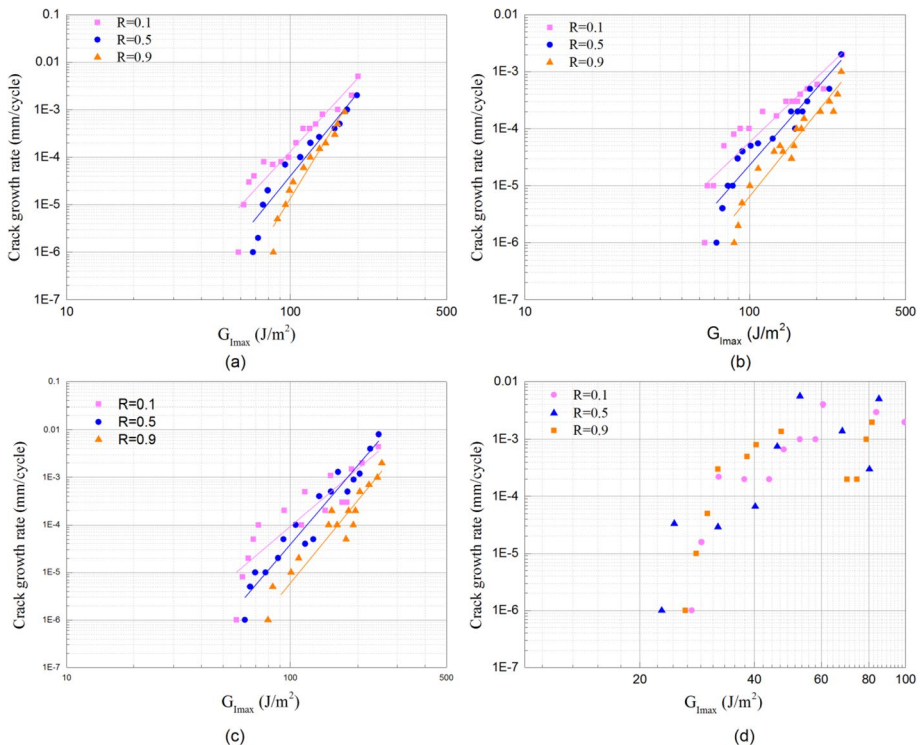


Fig. 7 FCG curves for **a** base laminate; **b** 0.05% CNT laminate; **c** 0.1% CNT laminate; **d** 0.5% laminate

Table 3 The power law fitting parameters for Paris relation

Laminate	<i>R</i> ratio	Proportionality Constant <i>C</i>	Exponent <i>m</i>	Coefficient of determination <i>R</i> ²
Base	0.1	1.16E-15	5.1	0.903
	0.5	2.82E-17	6.1	0.923
	0.9	4.43E-21	7.7	0.926
0.05% CNT	0.1	1.63E-12	3.8	0.891
	0.5	1.97E-14	4.5	0.888
	0.9	1.03E-15	4.9	0.773
0.1% CNT	0.1	6.19E-14	4.5	0.924
	0.5	6.34E-16	5.4	0.877
	0.9	3.26E-16	5.3	0.818

It is evident that with the lesser amount of fiber bridging at higher *R*-ratios, the matrix resin deformed inelastically producing the irreversibility that is important in inflicting substantial fatigue damage, particularly more so when the interlaminar matrix is responsible for the stiffness of the composite in pure mode I tests. Therefore, on unloading the specimen at which the bridged fibers failed, and reloading to maximum displacement again changes the stress states in the resin in the immediate neighborhood of the broken fibers. The new surrounding bridged fibers again change the state at the crack tip supporting more load and resulting in much less fatigue damage at higher *R*-ratios. Subsequent application of the cyclic loads results in an accumulative process that causes crack propagation and fatigue failure of the composite.

Apart from the slope, the *R*-ratio also has an effect on the position of the FCG curves. The FCG curves moved towards right with increasing *R*-ratio which means increase in delamination growth rate since the slope decreased with increase in *R*-ratio irrespective of the type of laminate used. A steeper curve for higher *R*-ratios also corresponds to higher fatigue threshold. The fiber bridging occurred for all the specimens except the one laminate with 0.5 wt% CNT, independent of the *R*-ratio.

The FCG curves obtained from the fatigue test data of the nanofiller reinforced laminates are shown in Fig. 7(b–d). Before fiber bridging occurs, the elastic and stiff carbon fibers inhibit the inelastic deformation of the resin when the crack migrates into the adjacent layer. The localized inelasticity of the matrix increases with broken bridged fibers, as discussed above. If by interface modification a given resin is nanoreinforced with CNTs, the local inelastic strain in the resin at the crack front will be less extensive and intense, i.e., extended over a lesser volume since now nanofillers bridge the crack front. Consequently, the progression of crack in fatigue-failure will be restricted, resulting in more cyclic loads to failure.

The strong interfacial bond in a carbon epoxy laminate with 0.05 wt% CNTs results in relatively low crack growth rates, which also allows the corresponding fiber bridging to develop behind the crack tip. Consequently, fracture energy is increased to break the fibers behind the crack tip leading to more crack growth resistance. However, nanofillers also inhibit the formation of fiber bridging by preventing the crack to migrate to adjacent layer. Therefore, fatigue loading exhibited lower amount of fiber bridging as compared to the static case of loading. Presence of relatively scattered data in nanofiller reinforced laminates implies complex combined effect of nanofillers and fiber bridging.

A relatively weak interlaminar bond, with 0.1 wt % CNTs, led to more extensive crack growth rate from multiple weak points in the interface, which causes strain energy release at

the crack tip. A more unstable crack growth also inhibited the development of bridged fibers. However, the propensity to delamination growth has another consequence: the individual multiple cracks formed throughout the weak regions due to nanofiller agglomeration are easily coalesced in the interface, which causes failure from the presence of sufficient surface area needed for unstable growth as seen in laminates nanoreinforced with 0.1 wt % and 0.5 wt% CNTs. In conclusion, an FCG curve that, for a given growth rate, corresponds to a high value of applied R ratio showed a better resistance to delamination than one for which the applied R is much smaller (at the same rate). On the other hand, a low value of slope resulted in higher delamination growth rates at relatively low applied loads as the reduction in growth rate as the test progressed was much less at low R -ratios.

Due to highly scattered data in 0.5% CNT reinforced laminates, FCG curves could not be obtained. The growth rates are much higher in these laminates since most of the crack growth increment takes place in the initial 10000 cycles. For the extreme case of a defective bonding or a very weak fiber-matrix interlaminar bond with 0.5 wt% CNTs, the mode of failure progression in fatigue changed from a bridged crack growth process (i.e., CNT and fiber bridging) to an accretion of the widespread interlaminar failure process. This was caused by a spread of enhanced stress surface area from cracked matrix in the vicinity of the crack to larger surrounding regions. Development of a well-defined bridged crack (from nanofillers and fibers) would then be infeasible; instead, widespread unstable cracking will occur throughout the interlaminar region, as is the case with this laminate.

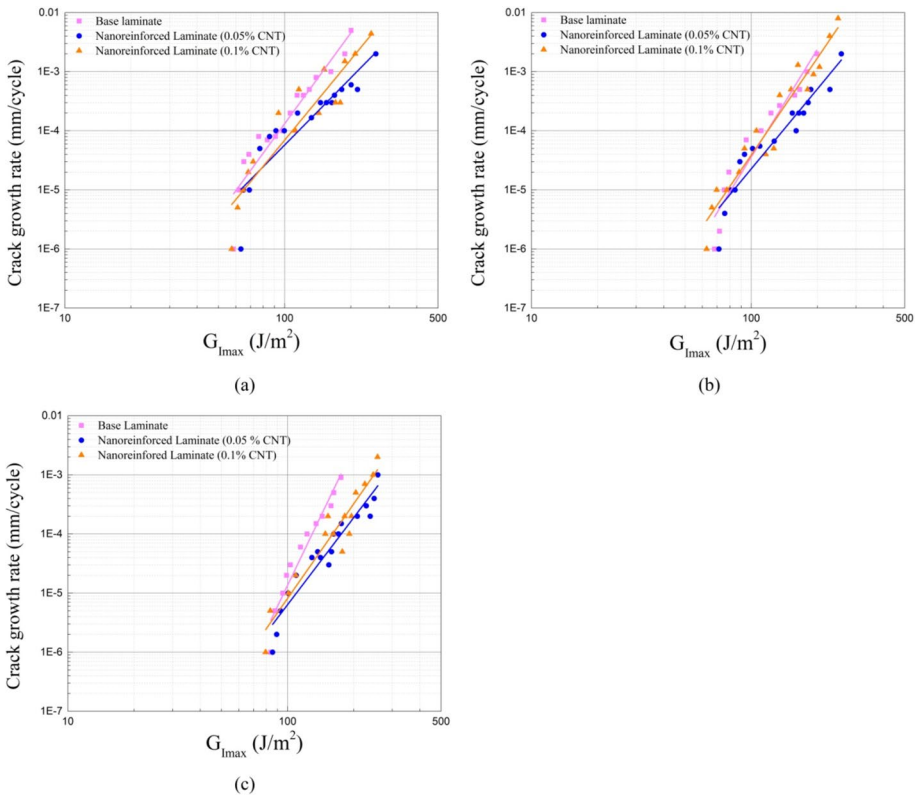


Fig. 8 FCG curves for various laminates **a** $R=0.1$; **b** $R=0.5$; **c** $R=0.9$

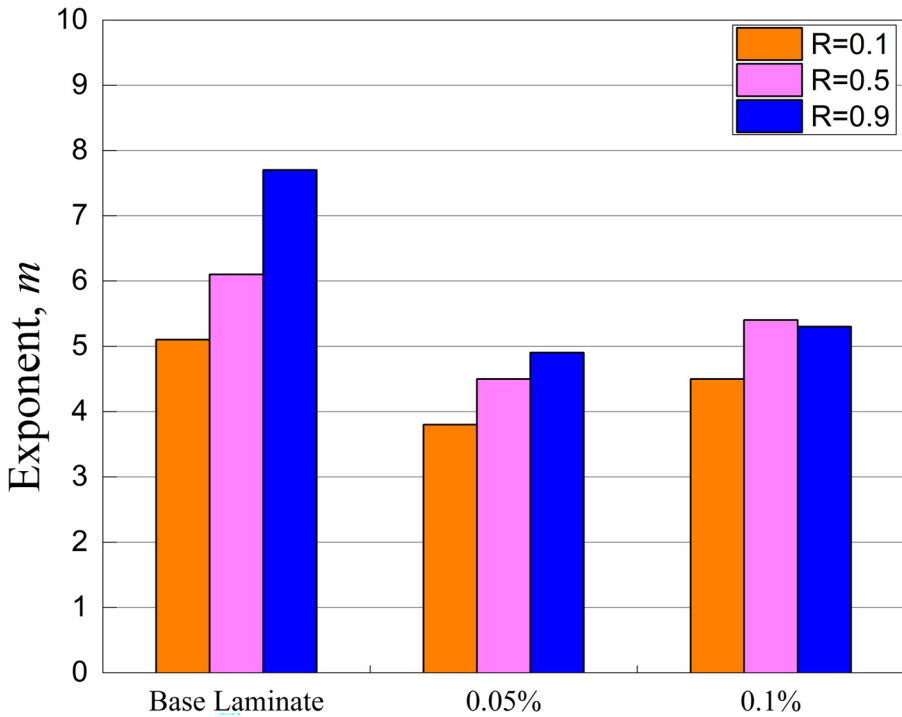


Fig. 9 Effect of stress ratio on the exponent m

The FCG curves are redrawn for each R -ratio to show the effect of each case of base laminate and nanoreinforced laminates, as shown in Fig. 8. In the present study it has been found that the use of nanofillers lowers the slope of FCG curves while still shifting the FCG curves to the right for higher R -ratios resulting in overall reduced FCG rate. An FCG curve with a steep slope implies significant increase in crack growth rate occurs for a small increment of the applied load (equivalent to G_{max}). Moreover, steep slopes result in large uncertainties in the prediction of crack growth rates (sometimes more than one decade) for relatively small changes in the applied load, i.e., change in da/dN is large enough to make the power-law relationships not useful. The large scatter in the slopes could also lead to uncertainties, if conservative growth rates are to be used in design. The effect of stress ratio on the slope m is illustrated in Fig. 9.

The FCG rate curves show that the exponents for relating delamination propagation rate to SERR are high for composites as compared to metals, especially in mode I [23, 35]. Typical slope values with different materials are given in Table 4. If the Paris relation is expressed in terms of K_{max} (where K is the stress-intensity factor), the corresponding da/dN

Table 4 Typical exponent values for various materials

Laminate	Exponent m
Steel	1.5–2
Aluminum	2–2.2
CFRP	5–10

Table 5 Average exponent values from the experimentation

Laminate	Exponent m
Base laminate	6.3
0.05% CNT laminate	4.4
0.1% CNT laminate	5.1

becomes proportional to $(K_{\max})^{12.6}$ for the base laminate since the G value is related to K^2 . This could lead to large errors (at least one order of magnitude) in the prediction of crack growth rates and therefore making the power law relationships with large slope values not suitable for design of structures. The average values of exponent m from the present study at different R -ratios are listed in Table 5.

4.2.1 Characterization of Fatigue Delamination Growth

There are various critical applications that cannot rely upon Paris relation due to the uncertainties in the prediction of da/dN . As discussed earlier, an FCG curve with a steep slope implies a significant increase in crack growth rate for a small increment of the applied load (equivalent to $G_{I_{max}}$). Moreover, steep slopes result in large uncertainties in the prediction of crack growth rates (sometimes more than one decade) for relatively small changes in the applied load, i.e., change in da/dN is large enough to make the power-law relationships not useful. The large scatter in the slope leads to uncertainties, if conservative growth rates are used in design. Threshold values obtained in a “no-growth” design can be used as an alternative to damage tolerant design philosophy. However, accurate determination of fatigue threshold may require longer test times, especially when low frequencies have to be chosen for large displacements. Moreover, if the tests were to be extended indefinitely it is unclear whether such threshold values exist or whether they are the result of limited experimental measurement resolution [24, 25]. In a study on ascertaining the threshold value after testing close to two million cycles, it was found that delamination length and compliance never reached an asymptotic value with virtually zero slope that would indicate the existence of the fatigue threshold [49].

Each of the Paris relation based FCG curves for different R -ratios were analyzed and re-plotted using the Hartman-Schijve correlation. The fitting parameters D and n for the FCG plots of Hartman-Schijve correlation are presented in Table 6.

The Hartman-Schijve correlation used in this study, considers all the data points that belong to different R -ratios to plot a single master curve. Data points for different

Table 6 The power law fitting parameters for Hartman-Schijve equation

Laminate	Stress ratio	D	n
Base laminate	0.1	3.78E-5	1.2
	0.5	1.85E-5	1.3
	0.9	9.92E-6	1.4
0.05% CNT	0.1	3.06E-5	1.2
	0.5	1.13E-5	1.2
	0.9	5.27E-6	1.3
0.1% CNT	0.1	2.4E-5	1.3
	0.5	1.41E-5	1.4
	0.9	1.56E-5	1.2

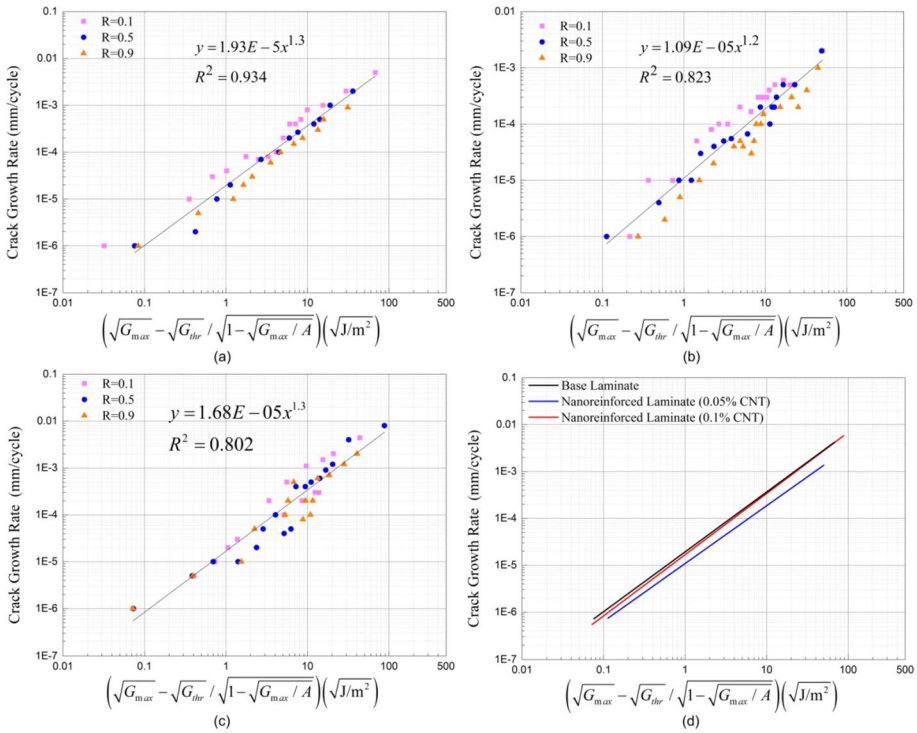


Fig. 10 The Hartman–Schijve representation of the Mode I fatigue behaviour for **a** base laminate; **b** 0.05% CNT laminate; **c** 0.1% CNT laminate; **d** Fitted curves shown together

R-ratios of the individual laminate are collapsed onto a single curve by using the power law fitting based on Harman-Schijve correlation, as shown in Fig. 10. The Hartman-Schijve proposes that all the data points can be represented by a single master curve if the threshold value is known. The exponent *n* is dependent on the threshold values. Therefore, its values in the current study are identical since threshold values do

Table 7 Threshold values G_{thr} used to obtain fitted FCG curves and design threshold to obtain upper-bound FCG curves

Laminate	<i>R</i> ratio	Fitting value <i>A</i> (J/m ²)	G_{thr}	Average G_{thr} (J/m ²)	Standard deviation G_{thr} (J/m ²)	Design G_{thr} (J/m ²)
Base	0.1	212.81	58.27	69.51	12.52	44.47
	0.5	204.68	67.27			
	0.9	181.24	83.00			
0.05 wt% CNT	0.1	275.44	63.11	73.01	9.54	53.93
	0.5	269.82	73.79			
	0.9	270.78	82.14			
0.1 wt% CNT	0.1	181.24	56.67	65.75	11.47	42.81
	0.5	252.71	61.94			
	0.9	270.78	78.64			

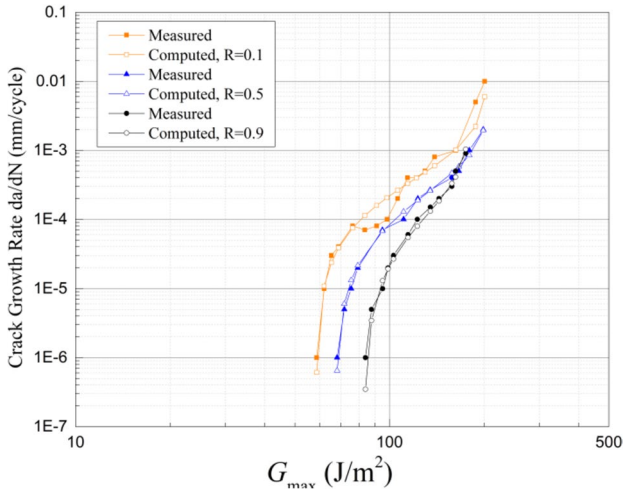


Fig. 11 The measured and computed Mode I fatigue behaviour for base laminate

not differ much. The fitted curves for base and nanoreinforced laminates, as shown in Fig. 10(d), reveal that the composites with 0.05 wt% CNTs provide better design curves for delamination resistance, and the curves for base laminate and 0.1 wt% CNT composites essentially overlap. With Hartman-Schijve correlation, the difference between design curves of base laminate and 0.1 wt% CNT composites seem minimal because of the identical design threshold values, as shown in Table 7.

The design threshold was calculated using a lower bound of twice the standard deviation on a normal distribution curve. The mean minus two standard deviations is equivalent to a 95% confidence estimate. This implies 95% of threshold values would lie in this range. Table 7 shows the design values (Average $G_{thr} - 2\sigma$) of G_{thr} , where σ is the standard deviation. Using such a procedure, a no-growth design can also be utilized by obtaining upper bound curves when a suitable design threshold is defined using standard deviation.

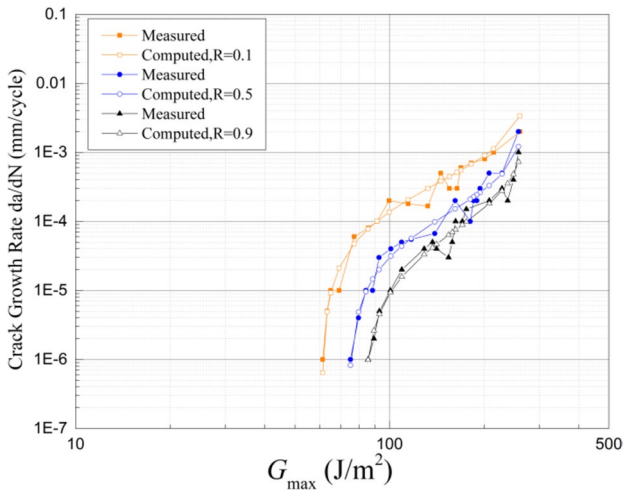


Fig. 12 The measured and computed Mode I fatigue behaviour for 0.05% CNT laminate

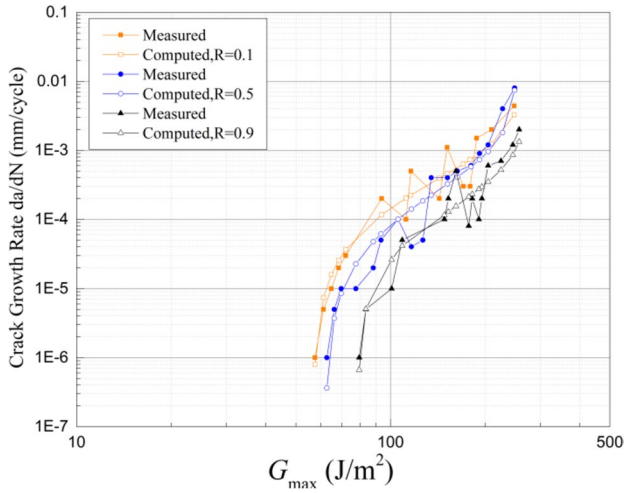


Fig. 13 The measured and computed Mode I fatigue behaviour for 0.1% CNT laminate

4.2.2 Evaluation of Crack Growth Rates

Crack growth rates were computed using Hartman-Schijve correlation by using the values of A and G_{thr} given in Table 7. These numerical evaluated results signify the validity of the

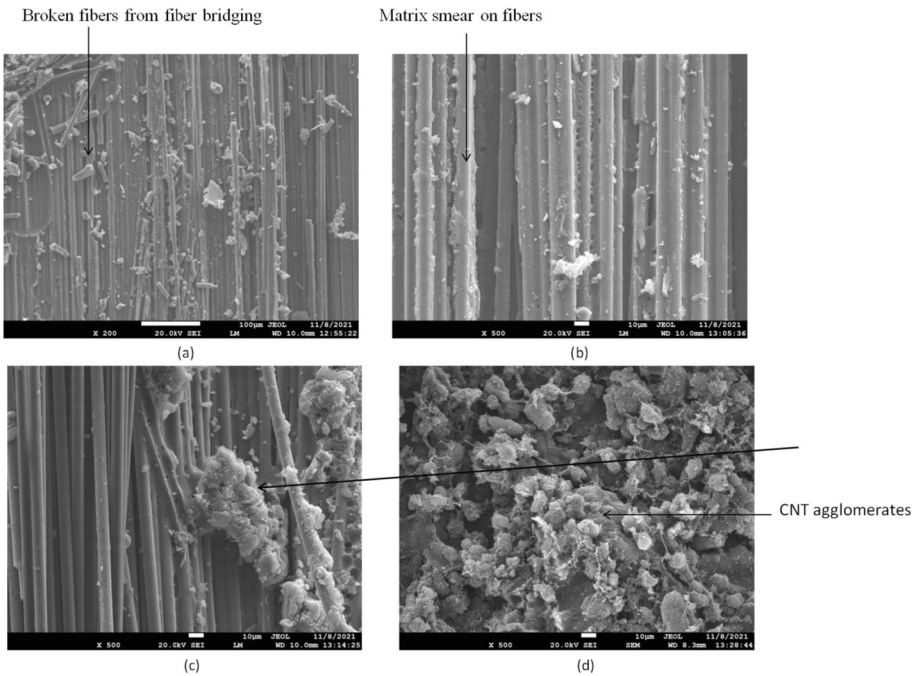


Fig. 14 SEM of the delamination fracture surface **a** base laminate (0.0% wt CNTs); **b** 0.05% CNT laminate; **c** 0.1% CNT laminate; **d** 0.5% CNT laminate

applied methodology of Hartman-Schijve to make predictions of crack growth rates. These predicted results were compared with the experimental results for every R -ratio studied.

The base laminates exhibit the smallest differences between the measured and computed responses as compared to laminated reinforced with nanofillers. The unstable crack growth is the major factor responsible for such behaviour since the abrupt changes in crack growth rate is not uncommon, especially in nanofiller reinforced laminates. Therefore, the predictions show slight discrepancy whenever there is abrupt change in da/dN . However the difference is less than half a decade on a double logarithmic scale. Crack growth rates were computed using Hartman-Schijve correlation, as shown in Figs. 11, 12 and 13.

5 Fracture Surface Study

Fractured surfaces of specimens containing 0.0 wt%, 0.05 wt%, 0.1 wt%, and 0.5 wt% CNTs were examined using scanning electron microscopy, as shown in Fig. 14. In base laminates (0.0 wt% CNTs), delamination occurs due to a combination of fiber/matrix debonding, matrix deformation and cracking. The surface of the base specimen displayed bare debonded fibers, with little or no epoxy attached to the fibers, which indicate failure along the fiber-matrix interface. This implies that it is predominantly adhesive failure mechanism at the interface which is associated with low resistance to crack propagation. The bridged fibers at the interface behind the crack tip provide additional delamination resistance at the crack tip.

With the addition of nanofillers, additional energy consumption mechanisms provide increased resistance against delamination propagation. The fracture surface of 0.05 wt% nanofiller reinforced laminate looks rougher with some nanofiller reinforced matrix smearing the fiber surface indicating toughening of the interface by better fiber-matrix adhesion. Bridging by nanofillers which results in pull-out and void growth provided additional extrinsic toughening of the interface. This shows that the 0.05 wt% CNTs provided enhanced fiber-matrix adhesion and extrinsic mechanisms in these laminates which contributed to energy absorption mechanisms. In 0.1 wt% carbon-nanotube reinforced laminate, agglomeration of carbon nanotubes in some regions, resulted in more pronounced stick slip behaviour as discussed earlier. This behavior results from the variation of interlaminar toughness since CNT agglomerates can be seen at fiber/matrix interface and which leads to preferential fracture in such zones and a local reduction in toughness resulting in erratic crack propagation seen in load–displacement curves. For 0.5 wt% nanofiller reinforced laminates, the interfacial bond between the fibers and the resin is deteriorated due to significant agglomeration of nanofillers. This resulted in poor consolidation of interlaminar region such that initiation fracture toughness and propagation fracture toughness were reduced significantly.

6 Conclusions

CFRP composites were experimentally characterized for mode I crack propagation under static and fatigue to study the effect of incorporating MWCNTs at the laminate interface. Three contents of MWCNTs (0.05 wt%, 0.1 wt%, and 0.5 wt%) were examined for quasi-static fracture by evaluating the fracture energy on initiation and propagation. The quasi-static tests were followed by interlaminar fatigue tests to characterize the delamination

growth under various R -ratios. For the prediction the crack growth rates, the effects of an (a) R -ratio, and (b) the variability seen in crack propagation of both base and nano-filler reinforced laminates have to be considered to characterize the fatigue failure. Therefore, master FCG curves were obtained which represent all the experimental data and which is representative of a laminate exhibiting these effects. The valid master curves can be used for the design of in-service composite components, the characterization and comparison of composite materials, for evaluating if in-service delamination will grow or not, and a 'no growth' design based on upper bound curves by defining a suitable design threshold using standard deviation. This methodology may also be helpful in the damage tolerant analysis of small naturally occurring defects in composite laminates.

The findings from the present study are summarized as:

- Multiscale composites exhibited a higher value of interlaminar initiation and propagation delamination resistance than base CFRP composites fabricated with neat epoxy. The experimental results indicated that the enhancement in the fracture toughness of CFRP composites can be achieved at a very low CNT concentration of 0.05%. The experimental results show a 50% and 48.54% increase in the interlaminar fracture toughness of the 0.05 wt% and 0.1 wt% MWCNTs content specimens, respectively as compared with base CFRP specimens.
- There is a critical CNT content above which the fracture toughness begins to deteriorate due to the limitation of the spraying technique to ensure uniform distribution and prevention of agglomeration of CNTs at large concentrations. Reduction of 49.19% in G_{IC} was observed for specimens incorporating 0.5 wt% CNTs, compared with base CFRP specimens.
- The addition of CNTs partially affects the FCG curves, with the effect being noticeable at low cyclic region, i.e. at high da/dN values. As the test gradually progresses the effect gradually diminishes as the various FCG curves in high cyclic region are closer to each other.
- At higher da/dN values, the fatigue fracture characteristics are similar to quasi-static fracture. This means lower strain energy dissipation during the initial fatigue crack growth as compared to quasi-static loading, which explains the effect of nanofillers. This effect diminishes at intermediate and lower values of da/dN , making nanofillers ineffective in high cyclic range.
- To account for the stress ratio effect Hartman-Schijve equation was used that gives a unique master curve with a low value of slope, n . The dependence of slope n on the fatigue threshold underlines the importance of accurate evaluation of it for design purposes. The findings from this study suggest that CFRP composite laminates fabricated with 0.05–0.1 wt.% nanofiller content provide enhanced delamination resistance under mode I quasi-static loading and improvement in FCG resistance in low cyclic fatigue.

Author Contributions Millan Kumar – Conceptualization, Methodology, Analysis, Data curation and Writing original draft, Review & Editing. Pramod Kumar – Conceptualization, Methodology, Writing – Review & Editing, Supervision. Shailendra Singh Bhadauria – Methodology, Writing – Review and Editing, Supervision.

Funding No funding was received for this work.

Data Availability The raw/processed data required to reproduce these findings cannot be shared at this time as the data also forms part of an ongoing study.

Declarations

Conflict of Interest The authors declare that they have no conflict of interest.

References

1. Fernández, M.V.C.: Fracture characterization of composite bonded joints under fatigue loading, Ph. D. Thesis, University of Porto, Portugal (2013)
2. Hojo, M., Tanaka, K., Gustafson, C.G.: Effect of stress ratio on near-threshold propagation of delamination fatigue cracks in unidirectional CFRP. *Composites* **19**, 329–330 (1988)
3. Andersons, J.: Empirical model for stress ratio effect on fatigue delamination growth rate in composite laminates. *Int. J. Fatigue* **26**, 597–604 (2004)
4. Hojo, M., Ando, T., Tanaka, M., Adachi, T., Ochiai, S., Endo, Y.: Modes I and II interlaminar fracture toughness and fatigue delamination of CF/epoxy laminates with self-same epoxy interleaf. *Int. J. Fatigue* **28**(10), 1154–1165 (2006)
5. Khan, R., Alderliesten, R., Badshah, S., Benedictus, R.: Effect of stress ratio or mean stress on fatigue delamination growth in composites: Critical review. *Compos. Struct.* **124**, 214–227 (2015)
6. Simon, I., Banks-Sills, L., Fourman, V.: Mode I delamination propagation and R-ratio effects in woven composite DCB specimens for a multi-directional layup. *Int. J. Fatigue* **96**, 237–251 (2017)
7. Arai, M., Noro, Y., Sugimoto, K.I., Endo, M.: Mode I and mode II interlaminar fracture toughness of CFRP laminates toughened by carbon nanofiber interlayer. *Compos. Sci. Technol.* **68**, 516–525 (2008)
8. Naik, N.K., Reddy, K.S., Meduri, S., Raju, N.B., Prasad, P.D., Azad, S.N.M., Ogde, P.A., Reddy, B.C.K.: Interlaminar fracture characterization for plain weave fabric composites. *J. Mater. Sci.* **37**, 2983–2987 (2002)
9. Fanteria, D., Lazzeri, L., Panettieri, E., Mariani, U., Rigamonti, M.: Experimental characterization of the interlaminar fracture toughness of a woven and a unidirectional carbon/epoxy composite. *Compos. Sci. Technol.* **142**, 20–29 (2017)
10. de Moura, M.F.S.F., Campilho, R.D.S.G., Amaro, A.M., Reis, P.N.B.: Interlaminar and intralaminar fracture characterization of composites under mode I loading. *Compos. Struct.* **92**, 144–149 (2010)
11. de Morais, A.: Mode-I interlaminar fracture of carbon/epoxy cross-ply composites. *Compos. Sci. Technol.* **62**, 679–686 (2002)
12. de Moura, M.F.S.F., Pereira, A.B., de Morais, A.B.: Influence of intralaminar cracking on the apparent interlaminar mode I fracture toughness of cross-ply laminates. *Fatigue Fract. Eng. Mater. Struct.* **27**, 759–766 (2008)
13. Brunner, A.J.: Experimental aspects of Mode I and Mode II fracture toughness testing of fibre-reinforced polymer-matrix composites. *Comput. Methods Appl. Mech. Eng.* **185**, 161–172 (2000)
14. de Morais, A.B., de Moura, M.F.S.F.: Evaluation of initiation criteria used in interlaminar fracture tests. *Eng. Fract. Mech.* **73**, 2264–2276 (2006)
15. de Morais, A.B.: Analysis of mode II interlaminar fracture of multidirectional laminates. *Compos. A Appl. Sci. Manuf.* **35**, 51–57 (2004)
16. Mathews, M., Swanson, S.: Characterization of the interlaminar fracture toughness of a laminated carbon/epoxy composite. *Compos. Sci. Technol.* **67**, 1489–1498 (2007)
17. Davidson, B.D., Gharibian, S.J., Yu, L.: Evaluation of energy release rate-based approaches for predicting delamination growth in laminated composites. **105**, 343–365 (2000)
18. Reeder, J.R., Rews, J.H.: Mixed-mode bending method for delamination testing. *AIAA J.* **28**, 1270–1276 (1990)
19. Benzeggagh, M.L., Kenane, M.: Measurement of mixed-mode delamination fracture toughness of unidirectional glass/epoxy composites with mixed-mode bending apparatus. *Compos. Sci. Technol.* **56**, 439–449 (1996)
20. Christensen, R.M., DeTeresa, S.J.: Delamination Failure Investigation for Out-of-plane Loading in Laminates. *J. Compos. Mater.* **38**, 2231–2238 (2004)
21. Pereira, A.B., de Morais, A.B.: Mode I interlaminar fracture of carbon/epoxy multidirectional laminates. *Compos. Sci. Technol.* **64**, 2261–2270 (2004)
22. Pereira, A.B., de Morais, A.B., Marques, A.T., de Castro, P.T.: Mode II interlaminar fracture of carbon/epoxy multidirectional laminates. *Compos. Sci. Technol.* **64**, 1653–1659 (2004)

23. Jones, R., Stelzer, S., Brunner, A.J.: Mode I, II and Mixed Mode I/II delamination growth in composites. *Compos. Struct.* **110**, 317–324 (2014)
24. Stelzer, S., Brunner, A.J., Argüelles, A., Murphy, N., Pinter, G.: Mode I delamination fatigue crack growth in unidirectional fiber reinforced composites: Development of a standardized test procedure. *Compos. Sci. Technol.* **72**, 1102–1107 (2012)
25. Stelzer, S., Brunner, A.J., Argüelles, A., Murphy, N., Cano, G.M., Pinter, G.: Mode I delamination fatigue crack growth in unidirectional fiber reinforced composites: Results from ESIS TC4 round-robins. *Eng. Fract. Mech.* **116**, 92–107 (2014)
26. Martin, R.H.: Interlaminar Fracture Characterization. *KEM.* **120–121**, 329–346 (1996)
27. Federal Aviation Authority.: Airworthiness advisory circular No: 20–107B. *Compos. Aircr. Struct.* (2009)
28. Yao, L., Alderliesten, R., Zhao, M., Benedictus, R.: Bridging effect on mode I fatigue delamination behavior in composite laminates. *Compos. A Appl. Sci. Manuf.* **63**, 103–109 (2014)
29. Murri, G.B.: Effect of data reduction and fiber-bridging on Mode I delamination characterization of unidirectional composites. *J. Compos. Mater.* **48**, 2413–2424 (2014)
30. RH, M., Murri, G.: Characterization of mode I and mode II delamination growth and thresholds in AS4/PEEK composites. In: Garbo P.S., *ASTM STP 1059*. pp. 251–270 (1990)
31. Jones, R., Kinloch, A.J., Michopoulos, J., Iliopoulos, A.P.: Crack growth in adhesives: Similitude and the Hartman-Schijve equation. *Compos. Struct.* **273**, 114260 (2021)
32. Jones, R., Kinloch, A.J., Michopoulos, J.G., Brunner, A.J., Phan, N.: Delamination growth in polymer-matrix fibre composites and the use of fracture mechanics data for material characterisation and life prediction. *Compos. Struct.* **180**, 316–333 (2017)
33. Brunner, A.J., Stelzer, S., Pinter, G., Terrasi, G.P.: Cyclic fatigue delamination of carbon fiber-reinforced polymer-matrix composites: Data analysis and design considerations. *Int. J. Fatigue* **83**, 293–299 (2016)
34. Jones, R., Hu, W., Kinloch, A.J.: A convenient way to represent fatigue crack growth in structural adhesives: characterising fatigue crack growth in structural adhesives. *Fatigue Fract. Eng. Mater. Struct.* **38**, 379–391 (2015)
35. Jones, R., Pitt, S., Bunner, A.J., Hui, D.: Application of the Hartman-Schijve equation to represent Mode I and Mode II fatigue delamination growth in composites. *Compos. Struct.* **94**, 1343–1351 (2012)
36. Rodríguez-González, J.A., Rubio-González, C., Meneses-Nochebuena, C.A., González-García, P., Licea-Jiménez, L.: Enhanced interlaminar fracture toughness of unidirectional carbon fiber/epoxy composites modified with sprayed multi-walled carbon nanotubes. *Compos. Interfaces* **24**, 883–896 (2017)
37. Zhang, H., Liu, Y., Kuwata, M., Bilotti, E., Peijs, T.: Improved fracture toughness and integrated damage sensing capability by spray coated CNTs on carbon fibre prepreg. *Compos. A Appl. Sci. Manuf.* **70**, 102–110 (2015)
38. Mujika, F., Vargas, G., Ibarretxe, J., De Gracia, J., Arrese, A.: Influence of the modification with MWCNT on the interlaminar fracture properties of long carbon fiber composites. *Compos. B* **43**, 1336–1340 (2012)
39. Shan, F.L., Gu, Y.Z., Li, M., Liu, Y.N., Zhang, Z.G.: Effect of deposited carbon nanotubes on interlaminar properties of carbon fiber-reinforced epoxy composites using a developed spraying processing. *Polym. Compos.* **16**, 41–50 (2013)
40. Almuhammadi, K., Alfano, M., Yang, Y., Lubineau, G.: Analysis of interlaminar fracture toughness and damage mechanisms in composite laminates reinforced with sprayed multi-walled carbon nanotubes. *Mater. Des.* **53**, 921–927 (2014)
41. Kumar, M., Kumar, P., Bhadauria, S.S.: Experimental characterization and numerical study on the interlaminar fracture toughness of carbon fibre reinforced polymer laminates reinforced with carbon nanotubes. *Materialwissenschaft Werkst.* **53**, 1561–1574 (2022)
42. Lubineau, G., Rahaman, A.: A review of strategies for improving the degradation properties of laminated continuous-fiber/epoxy composites with carbon-based nanoreinforcements. *Carbon* **50**, 2377–2395 (2012)
43. Davies, P., Blackman, B.R.K., Brunner, A.J.: Standard test methods for delamination resistance of composite materials: Current status. *Appl. Compos. Mater.* **5**, 345–364 (1998)
44. Qiu, J., Zhang, C., Wang, B., Liang, R.: Carbon nanotube integrated multifunctional multiscale composites. *Nanotechnology* **18**, 1–11 (2007)
45. Faulkner, S.D., Kwon, Y.W., Bartlett, S., Rasmussen, E.A.: Study of composite joint strength with carbon nanotube reinforcement. *J. Mater. Sci.* **44**, 2858–2864 (2009)
46. Joshi, S.C., Dikshit, V.: Enhancing interlaminar fracture characteristics of woven CFRP prepreg composites through CNT dispersion. *J. Compos. Mater.* **46**, 665–675 (2012)

47. Zhao, Y., Seah, L.K., Chai, G.B.: Measurement of interlaminar fracture properties of composites using the J-integral method. *J. Reinf. Plast. Compos.* **35**, 1143–1154 (2016)
48. Argüelles, A., Viña, J., Canteli, A.F., Bonhomme, J.: Fatigue delamination, initiation, and growth, under mode I and II of fracture in a carbon-fiber epoxy composite. *Polym. Compos.* **31**, 700–706 (2009)
49. Brunner, A.J., Murphy, N., Pinter, G.: Development of a standardized procedure for the characterization of interlaminar delamination propagation in advanced composites under fatigue mode I loading conditions. *Eng. Fract. Mech.* **76**, 2678–2689 (2009)
50. Grimmer, C.S., Dharan, C.K.H.: Enhancement of delamination fatigue resistance in carbon nanotube reinforced glass fiber/polymer composites. *Compos. Sci. Technol.* **70**, 901–908 (2010)
51. Arai, M., Hirokawa, J.-I., Hojo, M., Quaresimin, M.: Characteristic of mode I fatigue crack propagation of CFRP laminates toughened with CNF interlayer. *Compos. B Eng.* **65**, 19–24 (2015)
52. Kadlec, M., Šedek, J.: Fatigue delamination of a carbon fabric–reinforced epoxy composite with carbon nanotubes. *Compos. Sci. Technol.* **131**, 19 (2016)
53. Paris, P., Erdogan, F.: A Critical Analysis of Crack Propagation Laws. *J. Basic Engineering.* **85**, 528 (1963)
54. Jethwa, J.K., Kinloch, A.J.: The fatigue and durability behaviour of automotive adhesives. Part I: Fracture mechanics tests. *J. Adhes.* **61**, 71–95 (1997)
55. Ashcroft, I.A., Shaw, S.J.: Mode I fracture of epoxy bonded composite joints 2. Fatigue loading. *Int. J. Adhes. Adhes.* **22**, 151–167 (2002)
56. Amaral, L., Yao, L., Alderliesten, R., Benedictus, R.: The relation between the strain energy release in fatigue and quasi-static crack growth. *Eng. Fract. Mech.* **145**, 86–97 (2015). <https://doi.org/10.1016/j.engfracmech.2015.07.018>

Publisher's Note Springer Nature remains neutral with regard to jurisdictional claims in published maps and institutional affiliations.

Springer Nature or its licensor (e.g. a society or other partner) holds exclusive rights to this article under a publishing agreement with the author(s) or other rightsholder(s); author self-archiving of the accepted manuscript version of this article is solely governed by the terms of such publishing agreement and applicable law.